Simultaneous fitting of neutron star structure and cooling data

Spencer Beloin,[1] Sophia Han,[1,2,3] Andrew W. Steiner,[1,4] and Khorgolkhuu Odbadrakh[5]
[1]*Department of Physics and Astronomy, University of Tennessee, Knoxville, Tennessee 37996, USA*
[2]*Department of Physics and Astronomy, Ohio University, Athens, Ohio 45701, USA*
[3]*Department of Physics, University of California Berkeley, Berkeley, California 94720, USA*
[4]*Physics Division, Oak Ridge National Laboratory, Oak Ridge, Tennessee 37831, USA*
[5]*Joint Institute for Computational Sciences, Oak Ridge National Laboratory, Oak Ridge, Tennessee 37830, USA*

(Received 17 December 2018; revised manuscript received 16 September 2019; published 5 November 2019)

Using a model for the equation of state and composition of dense matter and the magnitude of singlet proton superconductivity and triplet neutron superfluidity, we perform the first simultaneous fit of neutron star masses and radii determined from observations of quiescent low-mass x-ray binaries and luminosities and ages determined from observations of isolated neutron stars. We find that the Vela pulsar strongly determines the values inferred for the superfluid/superconducting gaps and the neutron star radius. We find, regardless of whether or not the Vela pulsar is included in the analysis, that the threshold density for the direct Urca process lies between the central density of 1.7 and 2 solar mass neutron stars. We also find that two solar mass stars are unlikely to cool principally by the direct Urca process because of the suppression by neutron triplet superfluidity.

DOI: 10.1103/PhysRevC.100.055801

I. INTRODUCTION

The determination of the equation of state (EOS) of dense matter at densities beyond the saturation density has been dominated by the analysis of photon-based observations which lead to determinations of neutron star masses and radii [1–4]. The observation of gravitational waves from the binary neutron star merger GW170817 [5] by the LIGO-Virgo collaboration significantly changes this picture. Gravitational wave-based probes of the neutron star tidal deformability have smaller systematic uncertainties than electromagnetic probes of the neutron star radius [6]. Thus, depending on the mass distribution of progenitor masses of neutron stars that merge [7], gravitational wave observations can potentially drastically decrease the uncertainties in the EOS in the near future.

However, knowledge of the equation of state alone is insufficient to describe observed neutron star phenomenology. Neutron star cooling [8,9] and pulsar glitches [10] both depend strongly on the role played by superfluidity and superconductivity [11]. On the other hand, neither neutron star mass and radius observations nor gravitational wave detections are likely to constrain superfluidity or superconductivity in the near future. Thus, a joint analysis of data that constrains the EOS and the nature of pairing in dense matter is required to refine our understanding of neutron star observations.

In addition, determination of the equation of state does not ensure knowledge of the composition of dense matter. This was demonstrated in Ref. [12] where it was found that a mass-radius curve with neutrons and protons alone was nearly identical to that from a model containing deconfined quarks. Neutron star cooling, on the other hand, is sensitive to the neutron-to-proton ratio, since that controls the threshold for the direct Urca process [13,14].

Before this work, technical limitations forced quantitative analyses of neutron star masses and radii and neutron star thermal evolution to be almost entirely separate (for an exception, see Ref. [15]). In this work, we perform the first combined analysis of mass and radius data and luminosity and age data for isolated neutron stars with a well-defined likelihood function. In addition, we ensure that our model reproduces the structure of heavy nuclei. Since we allow the mass of each neutron star to vary, we can go beyond the "minimal cooling" model first envisaged in Ref. [9] by varying the EOS and including the direct Urca process.

II. METHOD

We presume that neutron stars contain only neutrons, protons, electrons, and muons, leaving the description of exotic hadrons or deconfined quarks to future work. We employ Bayesian inference, and all parameters below are taken to have uniform prior distributions. It is assumed that the data for each neutron star and all of the nuclear structure data are independent. The conditional probability (we will refer to this as the likelihood) will thus be a product of terms that we describe below.

Nuclei and the equation of state are modeled with a covariant field-theoretical Lagrangian from Ref. [16], based on earlier work in, e.g., Ref. [17]. To be as flexible as possible with regard to the description of high-density matter, the model in Ref. [16] (see Table 3 in Ref. [16]) used 17 parameters. We intentionally employ a relatively large parameter space to ensure that models are not prematurely ruled out. We compute

the structure of ^{208}Pb and ^{90}Zr in the Hartree approximation, and thus the first term in the likelihood is a Gaussian for the binding energy and charge radius of those two nuclei. We presume 2% uncertainties for the structure data, larger than the experimental accuracy, to allow for some systematics due to limitations in the Hartree approximation, similar to the method used in Refs. [16,18] (see also a similar calculation in Ref. [19]). We choose only one medium mass and one large mass nucleus because our goal is only to ensure that our nucleon-nucleon interaction is reasonable rather than to reproduce the properties of all nuclei. Pairing is not included in the nuclear structure calculations. We constrain the nuclear incompressibility to be between 220 and 260 MeV [20]. To be consistent with recent progress in nuclear theory, we restrict the symmetry energy at the nuclear saturation density, S, to be less than 36 MeV and the slope of the symmetry energy at the nuclear saturation density L to be less than 80 MeV [21]. A posterior correlation between S and L is automatically obtained from the fit to the nuclear structure data.

For the neutron star mass and radius data, we use the results obtained from the seven quiescent low-mass x-ray binary (QLMXB) neutron stars in the baseline data set from Refs. [22,23]. The associated term in the likelihood function is constructed as in, e.g., Eq. (102) of Ref. [21] (see also the more generic formalism developed in Ref. [24]). A nuisance variable is required to parametrize the curve, and we use the neutron star mass for this purpose, giving seven new parameters that are constrained to be larger than 1 solar mass. Each QLMXB (except for the neutron star in ω Cen) can have an atmosphere of either hydrogen or helium. We construct a new parameter η for each neutron star ranging between 0 and 1. If η is less than 2/3, then a hydrogen atmosphere is assumed, otherwise a helium atmosphere is assumed [22]. The only substantial difference between the mass and radius input from Ref. [22] and this work is the update of the M13 data as reported in Ref. [23].

For the isolated neutron star cooling data, we use the luminosity and age data from Table I of Ref. [25], and the associated term in the likelihood function is based on Eq. (4) of Ref. [25]. This data set does not include neutron stars with magnetic fields that are estimated to be larger than 10^{14} G, as the surface luminosity is more likely to be impacted by the magnetic field in these cases. We do not include the neutron stars in the Cassiopeia A ("Cas A") and HESS J1731−347 supernova remnants. The thermal evolution of the neutron star in Cas A is still not well understood (see Refs. [26–30]). XMMU J173203.3−344518 ("J1732") in HESS J1731−347 may be described by either a carbon atmosphere or a hydrogen atmosphere [31]. Finally, the carbon-atmosphere stars were shown to not have as strong an impact on the analysis as the Vela pulsar (PSR B0833−45; hereafter "Vela") does [25]. We also do not include the carbon-atmosphere stars CXOU J181852.0-150213 [32] and CXOU J160103.1-513353 [33] because pulsations have not permitted an age estimate. Below we present results with and without Vela due to its strong impact on the posteriors. Each of the 15 stars requires a mass parameter, and the 9 hydrogen-atmosphere stars may have a heavy- or light-element envelope, represented by the variable η [34] varying between 10^{-17} and 10^{-7} (note that this variable η from Ref. [34] refers to the composition of the envelope and differs from the variable η referred to in the preceding paragraph from Ref. [22], which refers to the atmosphere composition). We assume spherically symmetric surface temperatures and that the magnetic field is small enough to be irrelevant for the cooling.

All theoretical calculations of the singlet proton superconducting gap and the neutron triplet superfluid gap in the neutron star core contain uncontrolled approximations. Thus we parametrize the associated critical temperatures and allow the data to select the correct values, as in Ref. [25]. Each gap is described by a Gaussian function of the Fermi momenta, with height, centroid and width parameters denoted $T_{C,i}$, $k_{F,\mathrm{peak},i}$, and $\Delta k_{F,i}$, respectively. To avoid double-counting, for both neutrons and protons, we constrain $k_{F,\mathrm{peak}}$ to be larger than the value of k_F at the crust-core transition, and both $k_{F,\mathrm{peak}}$ and Δk_F to be smaller than the value of k_F in the core of the maximum-mass star. Note that we do not ensure that the superfluid or superconducting gaps are consistent with the Lagrangian used to describe the EOS of nucleonic matter. This kind of consistency, while sometimes important in nuclear structure [35], is unnecessary in this context since the pairing interaction does not strongly impact the equation of state and our gaps will always be less than 1 MeV, which is small compared to the nucleon Fermi energy. We include the direct Urca process, the modified Urca process, the pair-breaking neutrino emissivity, and other cooling processes enumerated in Refs. [9,36].

To account for the fact that our Lagrangian may not fully describe nucleons in the neutron star core, we add a two-parameter polytrope to our EOS following Ref. [37], which begins at twice the nuclear saturation density and either softens or stiffens the EOS depending on the sign of the coefficient and the magnitude of the exponent. We automatically reject any models that are acausal (because of the additional polytrope), have a maximum mass less than 2 $M_\odot$, or for which any neutron stars have a mass larger than the maximum mass of the EOS.

Our model has a total of 64 parameters, and traditional Bayesian inference applied to this problem requires the solution to the TOV equations, the nuclear structure calculations, and several cooling curves (to handle the variation in mass and envelope composition) at each point. To make it computationally tractable, we do not fully compute every point. Instead, we construct a library of exact calculations using a simple MCMC method. We fit the likelihood function to a 64-dimensional Gaussian (including covariances between all of the parameters) and then directly sample that Gaussian to generate parameter sets. To predict quantities other than the likelihood (cooling curves, M–R curves, gaps, etc.) from the library using samples from the Gaussian, we use inverse-distance-weighted interpolation. Sampling the emulator sometimes results in points which give unphysical values for the maximum mass or the speed of sound, so these points are removed to obtain the final results.

The full likelihood function is thus

$$\mathcal{L} = \mathcal{L}_{\mathrm{nuclei}}\mathcal{L}_{\mathrm{QLMXB}}\mathcal{L}_{\mathrm{INS}}\,. \tag{1}$$

The first term in Eq. (1) is the contribution from the nuclear structure data

$$\mathcal{L}_{\rm nuclei} = \exp\left[-\frac{\left(E_{\rm Zr}-\tilde{E}_{\rm Zr}\right)^2}{\left(0.02\tilde{E}_{\rm Zr}\right)^2}\right]\exp\left[-\frac{\left(R_{\rm Zr}-\tilde{R}_{\rm Zr}\right)^2}{\left(0.02\tilde{R}_{\rm Zr}\right)^2}\right] \times \exp\left[-\frac{\left(E_{\rm Pb}-\tilde{E}_{\rm Pb}\right)^2}{\left(0.02\tilde{E}_{\rm Pb}\right)^2}\right]\exp\left[-\frac{\left(R_{\rm Pb}-\tilde{R}_{\rm Pb}\right)^2}{\left(0.02\tilde{R}_{\rm Pb}\right)^2}\right], \quad (2)$$

where E_i is the calculated binding energy of nucleus i, $\tilde{E}_i$ is the experimental binding energy, R_i is the calculated charge radius, and $\tilde{R}_i$ is the experimental charge radius. The second term in Eq. (1) comes from the QLMXB observations

$$\mathcal{L}_{\rm QLMXB} = \prod_{i=1}^{7}\left\{\theta(2/3-\eta_i)\mathcal{D}_{i,\rm H}[R(M_i),M_i] + \theta(\eta_i-2/3)\mathcal{D}_{i,\rm He}[R(M_i),M_i]\right\}, \quad (3)$$

where i runs over the seven QLMXBs, η_i is the atmosphere parameter described above, M_i is the neutron star mass, $R(M_i)$ is the radius as a function of mass determined by the TOV equations, $\mathcal{D}_{i,\rm H}$ is the distance-uncertainty-averaged probability distribution obtained from the x-ray observations assuming a hydrogen atmosphere, and $\mathcal{D}_{i,\rm He}$ is the probability distribution assuming a helium atmosphere. The third term in Eq. (1) comes from the isolated neutron star (INS) cooling observations

$$\mathcal{L}_{\rm INS} = \prod_{j=1}^{16}\sum_{k}\sqrt{\left\{\left[\frac{d\widehat{L}(\eta_j,M_j)}{d\widehat{t}}\right]_k^2+1\right\}} \times \exp\left\{\frac{-\left[\widehat{t}_k-\widehat{t}_j\right]^2}{2(\delta\widehat{t}_j)^2}\right\} \times \exp\left\{\frac{-\left[\widehat{L}_k(\eta_j,M_j)-\widehat{L}_j\right]^2}{2(\delta\widehat{L}_j)^2}\right\}, \quad (4)$$

where j is an index over the 16 isolated neutron stars (or 15 if Vela is not included), $\widehat{t}=\log_{10}[t/(10^2\,\rm yr)]/5$ is a logarithmic coordinate for the time, $\widehat{L}=\log_{10}[L/(10^{30}\,\rm erg/s)]/4$ is a logarithmic coordinate for the luminosity, k is an index over a uniform grid in $\widehat{t}$ (see Ref. [25] for details), η_j is a parameter for the envelope composition which runs from 10^{-19} to 10^{-7}, $\widehat{L}_k(\eta_j,M_j)$ is the theoretical luminosity for neutron star j at grid point k (which depends on envelope composition and mass), $\widehat{L}_j\pm\delta\widehat{L}_j$ is the observed luminosity with its associated uncertainty, $\widehat{t}_j\pm\delta\widehat{t}_j$ is the observed age with its associated uncertainty, and the term under the square root is a geometric factor (see Ref. [24]). The computation of $\widehat{L}_k(\eta_j,M_j)$ requires first a solution of the TOV equations to determine the structure, and then a solution of the stellar evolution equations to determine the cooling.

III. RESULTS

The posterior distributions for the neutron and proton density distributions are given in Fig. 1(a). Regardless of whether or not Vela is included, the charge radii are within 2% of the experimental value of 5.5 fm. (As found in Ref. [25], Vela has a strong impact on the results because its luminosity is comparatively small given its estimated age.) Our 95% credible range for the neutron skin thickness of ^{208}Pb is 0.15 to 0.20 fm (0.143 to 0.157 fm) without (with) Vela. The addition of Vela pushes several parameters, including those which control the nucleon-nucleon interaction, to extreme values. When Vela is included, the value of L (and thus the value of the skin thickness) is pushed towards smaller values to decrease the specific heat and increase the cooling. Note that when L is smaller, the isospin asymmetry in the central region increases to ensure that the total neutron and proton number is fixed [16].

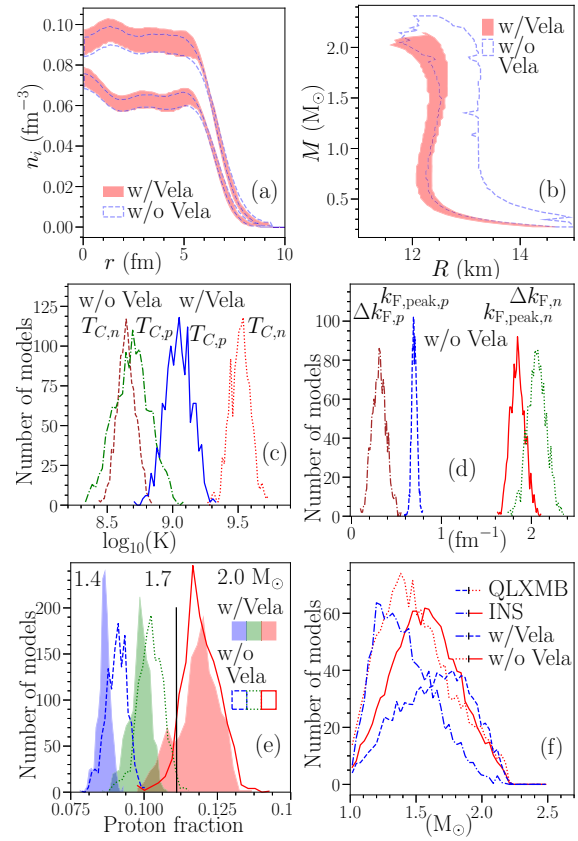

FIG. 1. All panels except (d) show results with and without Vela. For display purposes, simulations with and without Vela are fixed to have the same overall normalization. Panel (a): 95% credible intervals for the neutron and proton density profiles for ^{208}Pb. Panel (b): 95% credible intervals for the mass-radius curves. Panel (c): histograms for the maximum value of the proton singlet and neutron triplet gaps. Panel (d): Histograms for the other two gap parameters for neutrons and protons for the analysis excluding Vela. Panel (e): Histograms for the central proton fraction of 1.4, 1.7, or 2.0 $M_\odot$ neutron stars. Panel (f): Posterior mass distributions for the seven QLMXB neutron stars or the 14 isolated cooling neutron stars (or 15 stars when Vela is included).

The distribution for mass-radius curves is plotted in Fig. 1(b). We find the radius of a 1.4 solar mass star to be between 12.4 and 13.1 km (12.35 to 12.65 km) without (with)

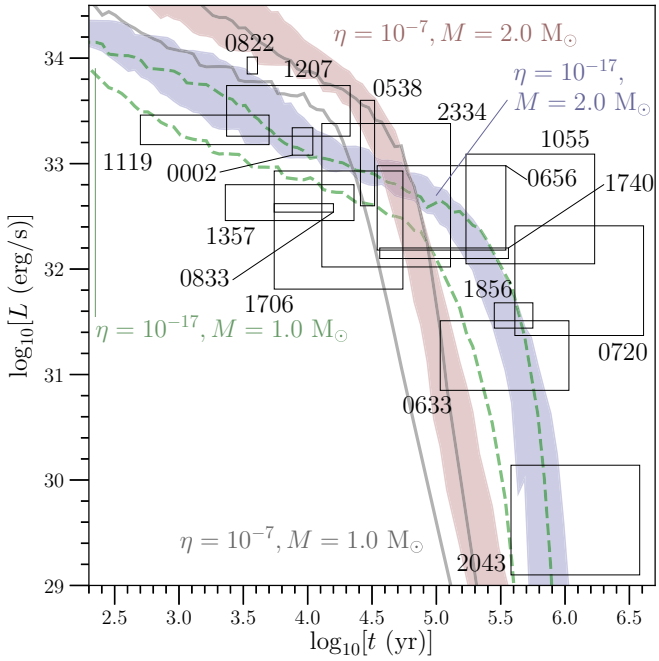

FIG. 2. The 95% credible intervals for the luminosity-age curves for different neutron star masses and different amounts of light elements in the neutron star envelope (parameterized by η), along with the luminosity and age values obtained from observations which were used in this work. Vela (labeled "0833") is not included in the model results but the data point is included in the figure for comparison.

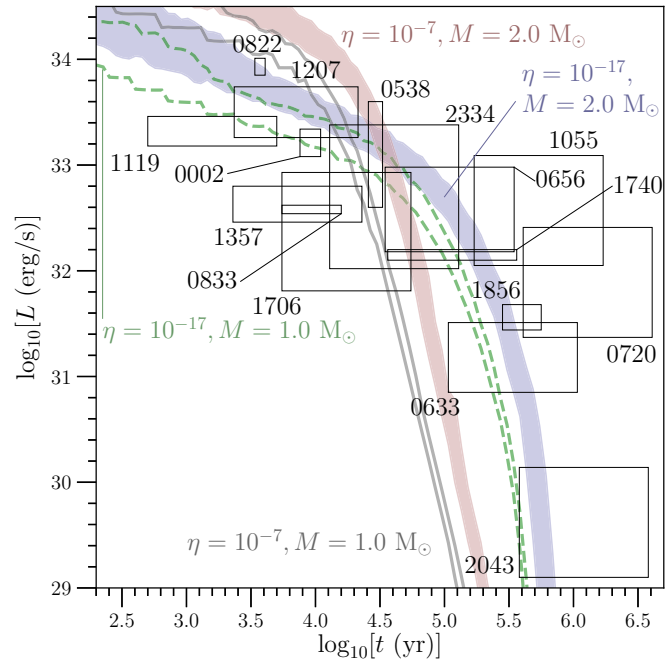

FIG. 3. The 95% credible intervals for the luminosity-age curves for different neutron star masses and different amounts of light elements in the neutron star envelope (parameterized by η), along with the luminosity and age values obtained from observations which were used in this work. Vela (labeled "0833") is included in the model results.

Vela. When Vela is included, the smaller value of L leads to smaller neutron star radii. These ranges are consistent with that obtained from QLMXBs alone (11.0 to 14.3 km) [22], and also with the radius inferred by the GW170817 merger (9.1 to 12.8 km) [38]. There is some jitter in the radius limits due to small statistics.

The peak values of critical temperatures for the proton and neutron superfluid are presented in Fig. 1(c). As in Ref. [25], we find significantly different results depending on whether or not Vela was included: the gaps are significantly larger when Vela is included, which helps maximize the neutrino emissivity from the breaking and formation of Cooper pairs [36,39–44]. (Note that, as shown in Fig. 6 of Ref. [36], the dependence of the cooling curve on the critical temperature is not monotonic.) Figure 1(d) shows the centroid and width parameters for the gaps without Vela. We find that $\Delta k_{F,n}$ is large with or without Vela, which effectively prevents the direct Urca process from occurring in the core. This is consistent with the observational data, as no confirmed isolated neutron stars have very low luminosities (see Figs. 2 and 3 below).

Figure 1(e) displays histograms for the proton fraction in the cores of 1.4, 1.7, and 2.0 $M_\odot$ neutron stars along with a vertical line at 11%, the threshold for nonsuperfluid neutrons and protons to participate in the direct Urca process when muons are ignored. We find it unlikely that 1.7 $M_\odot$ neutron stars have proton fractions larger than 11%, and very likely that all 2.0 $M_\odot$ stars do. Adding muons tends to decrease the critical density [14] for the Urca process to satisfy energy and momentum conservation. However, the neutron superfluid quenches the direct Urca process, even in 2.0 $M_\odot$ stars.

Figure 1(f) shows the mass posterior for the QLMXB and isolated neutron star (INS) data sets with Vela (dashed and dot-dashed lines) and without Vela (dotted and solid lines). Including Vela decreases the radius of all neutron stars (for fixed gravitational mass), as shown above. Since the QLMXB observations tend to fix $R_\infty = R/\sqrt{1-2GM/(Rc^2)}$, decreasing R tends to increase M. When Vela is not included, probability distributions for both QLMXBs and INSs peak near 1.4 $M_\odot$, similar to that observed in NS-NS and NS-WD binaries with accurate mass measurements [45]. The mass distributions here imply that QLMXBs are less massive than INSs when Vela is not included, backwards from what is expected since QLMXBs gain mass through accretion (see, e.g., Refs. [46,47]). However, the individual masses have large uncertainties so the precise locations of the peaks in Fig. 1 are not significant (see Appendix for details). More data will be required to definitively predict mass distributions in this way.

In Fig. 2, we show the luminosity-age cooling curves excluding Vela. The bands refer to the 95% credible regions for the luminosity as a function of age. Note that while the gravitational mass is presumed to be constant over the time period shown, the amount of light elements in the envelope, parameterized by η, may decrease over time as nuclear reactions fuse these light elements into heavier ones. Cooling curves with Vela included are plotted in Fig. 3. The uncertainty ranges are much smaller, demonstrating that a much smaller set of parameters is able to accommodate Vela's

small luminosity given its age. The larger mass stars cool slightly more slowly, as explained in Ref. [9] (see Fig. 25). As would be expected, our predicted mass for Vela is smaller, $1.25 \pm 0.25\,M_\odot$ to ensure a smaller luminosity for this object.

There are several other recent works describing the cooling of isolated neutron stars which analyze a smaller data set, and employ a smaller set of nucleon pairing models with a smaller set of EOS models, but often take into account exotic degrees of freedom. The authors of Ref. [48] studied stars containing hyperons and found a significant contribution from hyperonic direct Urca processes. The authors of Ref. [49] also studied stars containing hyperons and found small neutron star radii and large masses were preferred. The authors of Ref. [50] focused on magnetic fields, which we do not include, and were thus able to include magnetars in their analysis. The authors of Ref. [51] included a helpful analytical description of isolated neutron star cooling. The authors of Ref. [52] used a method similar to ours to analyze the cooling of J1732, and included the possibility of axion cooling. They applied a single EOS and found large proton and small neutron gaps.

IV. CONCLUSION AND DISCUSSION

In this work, we analyze the implications that our data set, which includes neutron star masses, radii and luminosity, and age determinations for isolated cooling neutron stars, have on dense matter. These data suggest that the direct Urca process is unlikely to play a prominent role in neutron star cooling because of suppression by neutron triplet superfluidity throughout the core. The proton fraction in dense matter is unlikely to remain below the threshold for energy and momentum conservation in the direct Urca process in the core of more massive neutron stars. The minimal cooling model [9] assumes that the direct Urca process does not occur, presuming that either the EOS does not the direct Urca process at any density inside neutron stars or that the mass of isolated neutron stars is not large enough to create a large central proton density. The results of this work suggest that superfluidity, rather than the EOS, suppresses the direct Urca process for low to moderate mass neutron stars.

Many-body correlations (see, e.g., Refs. [53–55]) at high densities can impact these neutrino processes and can impact our conclusions. However, it is difficult to include all possible models of these correlations and the additional uncertainty is difficult to quantify because the associated many-body calculations are not systematically improvable. We hope to include this in future work.

In this work we used a field-theoretical Lagrangian, but performing a similar analysis using a Skyrme model might also be instructive. However, Skyrme models are also likely to become acausal at densities below the central density of the maximum mass star [56]. As also found for mass and radius data alone in Refs. [4,57], we do expect our results to be sensitive to our prior choices, particularly with regard to the equation of state. We added an additional polytrope at high densities and the impact of the polytrope is estimated in the Appendix.

After completing this work we found that updated distance measurements in Ref. [58] will modify the luminosity inferred for B1706-44, which was reported in Ref. [25]. However, this modification is unlikely to modify our basic conclusions since the uncertainty in the luminosity for this source is large.

We find that the most likely models selected by this inference appear incompatible with the cooling of the coldest transiently accreting sources, such as SAX J1808.4−3658 [37,59]. The suppression of the direct Urca emissivity due to pairing found here cannot explain the low temperatures observed. However, this incompatibility may be resolved simply if all of the neutron stars in this work have smaller masses and if SAX J1808 has a large mass. The best way forward is to simultaneously fit both isolated and accreting neutron stars, in addition to the information from neutron star mass and radius determinations. Initial progress on simultaneous fitting of these two data sets has been made in Refs. [60,61] using a handful of EOSs.

The authors of Refs. [51,62] also examined the cooling of the Vela pulsar and similarly observed that it was cooling faster than most of the rest of the population. In contrast to our work, they used the x-ray spectrum directly to determine its mass and radius. They also found a relatively low mass for Vela, and they also found that it can be explained in the context of the minimal cooling model where the direct Urca process is ignored.

ACKNOWLEDGMENTS

We thank Dany Page for publicly releasing his NSCool neutron star cooling code. We also thank Craig Heinke and Joonas Nättilä for helpful discussions. This work was supported by NSF Grant No. PHY 1554876 and by the U.S. DOE Office of Nuclear Physics. S.H. is also supported by Chandra Grant No. TM8-19002X, NSF Grant No. PHY-1630782, and the Heising-Simons Foundation, Grant No. 2017-228. This work used the Extreme Science and Engineering Discovery Environment (XSEDE) allocation PHY170048 supported by NSF Grant No. ACI-1548562 and computational resources from the University of Tennessee and Oak Ridge National Laboratory's Joint Institute for Computational Sciences.

APPENDIX: FIT ANALYSIS

This data analysis problem consists of 22 (or 23 when Vela is included) neutron star observations and 4 nuclear structure data points, two constraints on the symmetry energy, one constraint on the incompressibility, and 64 parameters, and thus is formally underconstrained. Part of the reason the problem is underconstrained is the additional mass (nuisance) parameter required for each neutron star to map the location on the curve to the two-dimensional data point (as shown in Ref. [24]). However, not all of the parameters impact the fit equally. For the cooling neutron stars, the mass and the variable η which represents the composition of the envelope make only a small correction to the cooling curve (unless the direct Urca process is allowed, which we find is unlikely). In the midst of these complications, although we do not have the computational time to explicitly verify this, our problem is sufficiently underconstrained that we expect our prior choice

will impact our results, as found for QLMXBs and other neutron star observations in Ref. [4].

One of the biggest difficulties with a large parameter space is the possibility of overfitting. A complete analysis of overfitting requires a much more computationally intensive cross-validation which we cannot yet perform. One of the symptoms of overfitting is that the parameters are allowed to vary so widely that the model becomes physically unrealistic. In lieu of a full cross-validation, we discuss the posterior distributions of the parameters and show that they are within the expected range and that they do not have unreasonably small uncertainties. We find no reason to believe that overfitting is impacting the principal results in this paper, as described below.

The superfluid/superconducting critical temperatures which we obtain when Vela is not included closely match what was obtained previously in Ref. [9], and the fact that Vela has a particularly weak luminosity has also been observed elsewhere [51,62], thus it is unsurprising that our critical temperatures are modified when this neutron star is included. The other superfluid parameters are not frequently constrained in the literature, except in Ref. [15], which analyzed Cas A, so there is little guidance except from uncontrolled theory estimates. The posterior values for the envelope composition, as described in Ref. [25], are also reasonable given the relative location of the data points to the posterior cooling curves.

All of the posterior values for the neutron star masses are between 1.0 and 2.0 solar masses, as would be expected from the recent status of simulations of core-collapse supernovae [63,64]. All of the posterior mass distributions also have large uncertainties, between 0.15 and 0.35 solar masses. When Vela is not included, the lower-right panel implies that QLMXBs are about 0.1 $M_\odot$ less massive that the isolated neutron stars, but the uncertainty in the individual masses means that this is probably not significant. When Vela is included, the ordering is reversed, and QLMXBs are more massive, as might be expected from evolutionary considerations.

To assess the values of the interaction couplings, we compare them with the range of values covered by the SFHo [18], SFHx [18], SR1 [16], SR2 [16], SR3 [16], es25 [16], es275 [16], es30 [16], es325 [16], es35 [16], RAPR [16], NL3 [65], Z271 [66], S271 [66], NL4 [67], FSUGold [68], and IUFSU [69] models. We include several models from Ref. [16] because this paper contains several models with the same set of coupling constants. For each coupling (and also for the mass of the scalar meson, m_σ), for the results with and without Vela, we compute the quantity

$$X_q \equiv \frac{P_q - \min_q}{\max_q - \min_q}, \tag{A1}$$

where P_q is the peak of the posterior distribution for quantity q, and $\min_q$ and $\max_q$ are the minimum and maximum values across the models listed above. The posterior value is outside the range covered by the models only when $X < 0$ or $X > 1$. We find values only slightly outside [0,1]: a_3 and m_σ when Vela is included (see Table I) and for a_3 and a_4 when Vela is not included.

TABLE I. Comparison of posteriors for the parameters in our Lagrangian (given in Ref. [16]) with the ranges given by other models [see Eq. (A1)].

Quantity, q	$X_{q,\mathrm{w/Vela}}$	$X_{q,\mathrm{w/o\,Vela}}$
a_1	0.570	0.576
a_2	0.0168	-5.91×10^{-3}
a_3	−0.112	−0.0551
a_4	3.87×10^{-3}	−0.0545
a_5	8.61×10^{-4}	0.0318
a_6	0.0697	0.0792
b	0.0787	0.124
b_1	0.899	0.767
b_2	1.01	0.988
b_3	-3.33×10^{-4}	1.37×10^{-4}
c	0.248	0.196
c_ρ	0.977	0.937
c_σ	0.692	0.783
c_ω	0.718	0.777
m_σ	1.25	0.876
ξ	6.18×10^{-3}	-5.50×10^{-3}
ζ	0.499	0.362

These deviations are relatively small, but it is more straightforward to interpret physical observables. We find the saturation density of nuclear matter $0.155 \pm 0.005\,\mathrm{fm}^{-3}$ (with Vela) and $0.152 \pm 0.004\,\mathrm{fm}^{-3}$ (without Vela) are both in the empirical range [70]. The binding energy at saturation is -16.32 ± 0.31 MeV (with Vela) and -16.34 ± 0.32 MeV are in the empirical range as well.

The additional polytrope, $P = K\,\varepsilon^\Gamma$, is more unusual, so we estimate the impact that this additional polytrope has on the principal results of the paper. The posterior distribution for K is 0.134 ± 0.045 (with Vela) and 0.100 ± 0.047 (without Vela). The Pearson correlation coefficient between K and several quantities from the simulation are given in Table II. When Vela is included, decreasing K to zero (and thus removing the polytrope) will tend to decrease $k_{F,\mathrm{peak},p}$, and increase the proton fraction which may allow the direct

TABLE II. Pearson correlation coefficients for various quantities and the polytrope coefficient. The first six quantities are the parameters for the critical temperatures described in the method section above, x is the proton fraction at the specified density, and the last row shows the correlation with the neutron star maximum mass.

Quantity	$C(q,K)_{\mathrm{w/Vela}}$	$C(q,K)_{\mathrm{w/oVela}}$
$T_{C,n}$	−0.0283	0.15
$k_{F,\mathrm{peak},n}$	−0.143	0.596
$\Delta k_{F,n}$	−0.179	0.534
$T_{C,p}$	−0.0765	0.0189
$k_{F,\mathrm{peak},p}$	−0.451	−0.11
$\Delta k_{F,p}$	0.133	0.155
$x_{n=n_0}$	0.223	0.429
$x_{n=2n_0}$	0.206	0.057
$x_{n=3n_0}$	0.158	−0.148
$M_{\max}$	0.912	0.543

Urca process to proceed in more massive stars. When Vela is not included, decreasing K to zero will tend to increase both $k_{F,\mathrm{peak},n}$ and $\Delta k_{F,n}$ which will not have a strong impact. Since the polytrope modifies the high-density behavior, a correlation with the neutron star maximum mass, $M_{\max}$ is expected. Thus, removing the polytrope would modify the couplings of nuclear interaction, but those modifications are limited because of the constraints that we used.

[1] A. G. Cameron, Astrophys. J. **130**, 884 (1959).
[2] J. M. Lattimer and M. Prakash, Astrophys. J. **550**, 426 (2001).
[3] A. W. Steiner, J. M. Lattimer, and E. F. Brown, Astrophys. J. **722**, 33 (2010).
[4] A. W. Steiner, J. M. Lattimer, and E. F. Brown, Astrophys. J. Lett. **765**, 5 (2013).
[5] B.P. Abbott *et al.* (LIGO Scientific Collaboration and Virgo Collaboration), Phys. Rev. Lett. **119**, 161101 (2017).
[6] B. D. Lackey and L. Wade, Phys. Rev. D **91**, 043002 (2015).
[7] C. L. Fryer, K. Belczynski, E. Ramirez-Ruiz, S. Rosswog, G. Shen, and A. W. Steiner, Astrophys. J. **812**, 1 (2015).
[8] D. Yakovlev and C. Pethick, Annu. Rev. Astron. Astrophys. **42**, 169 (2004).
[9] D. Page, J. M. Lattimer, M. Prakash, and A. W. Steiner, Astrophys. J. Suppl. Ser. **155**, 623 (2004).
[10] J. Piekarewicz, F. J. Fattoyev, and C. J. Horowitz, Phys. Rev. C **90**, 015803 (2014).
[11] D. Page, J. M. Lattimer, M. Prakash, and A. W. Steiner, in *Novel Superfluids*, Vol. 2 (Oxford University Press, Oxford, 2014), p. 505.
[12] M. Alford, M. Braby, M. Paris, and S. Reddy, Astrophys. J. **629**, 969 (2005).
[13] J. Boguta, Phys. Lett. B **106**, 255 (1981).
[14] J. M. Lattimer, C. J. Pethick, M. Prakash, and P. Haensel, Phys. Rev. Lett. **66**, 2701 (1991).
[15] W. C. G. Ho, K. G. Elshamouty, C. O. Heinke, and A. Y. Potekhin, Phys. Rev. C **91**, 015806 (2015).
[16] A. W. Steiner, M. Prakash, J. M. Lattimer, and P. J. Ellis, Phys. Rep. **411**, 325 (2005).
[17] B. D. Serot and J. D. Walecka, Adv. Nucl. Phys. **16**, 1 (1986), https://www.worldcat.org/isbn/9780306419973.
[18] A. W. Steiner, M. Hempel, and T. Fischer, Astrophys. J. **774**, 17 (2013).
[19] W.-C. Chen and J. Piekarewicz, Phys. Rev. C **90**, 044305 (2014).
[20] U. Garg and G. Coló, Prog. Part. Nucl. Phys. **101**, 55 (2018).
[21] J. M. Lattimer and A. W. Steiner, Eur. Phys. J. A **50**, 40 (2014).
[22] A. W. Steiner, C. O. Heinke, S. Bogdanov, C. Li, W. C. G. Ho, A. Bahramian, and S. Han, Mon. Not. R. Astron. Soc. **476**, 421 (2018).
[23] A. W. Shaw, C. O. Heinke, A. W. Steiner, S. Campana, H. N. Cohn, W. C. G. Ho, P. M. Lugger, and M. Servillat, Mon. Not. R. Astron. Soc. **476**, 4713 (2018).
[24] A. W. Steiner, arXiv:1802.05339.
[25] S. Beloin, S. Han, A. W. Steiner, and D. Page, Phys. Rev. C **97**, 015804 (2018).
[26] D. Page, M. Prakash, J. M. Lattimer, and A. W. Steiner, Phys. Rev. Lett. **106**, 081101 (2011).
[27] P. S. Shternin, D. G. Yakovlev, C. O. Heinke, W. C. G. Ho, and D. J. Patnaude, Mon. Not. R. Astron. Soc. Lett. **412**, 108 (2011).
[28] A. Bonanno, M. Baldo, G. F. Burgio, and V. Urpin, Astron. Astrophys. **561**, L5 (2014).
[29] K. G. Elshamouty, C. O. Heinke, G. R. Sivakoff, W. C. G. Ho, P. S. Shternin, D. G. Yakovlev, D. J. Patnaude, and L. David, Astrophys. J. **777**, 22 (2013).
[30] B. Posselt, G. G. Pavlov, V. Suleimanov, and O. Kargaltsev, Astrophys. J. **779**, 186 (2013).
[31] D. Klochkov, V. Suleimanov, G. Pühlhofer, D. G. Yakovlev, A. Santangelo, and K. Werner, Astron. Astrophys. **573**, A53 (2015).
[32] D. Klochkov, V. Suleimanov, M. Sasaki, and A. Santangelo, Astron. Astrophys. **592**, L12 (2016).
[33] V. Doroshenko, V. Suleimanov, and A. Santangelo, Astron. Astrophys. **618**, A76 (2018).
[34] A. Y. Potekhin, G. Chabrier, and D. G. Yakovlev, Astron. Astrophys. **323**, 415 (1997).
[35] W.-C. Chen, J. Piekarewicz, and A. Volya, Phys. Rev. C **89**, 014321 (2014).
[36] D. Page, J. M. Lattimer, M. Prakash, and A. W. Steiner, Astrophys. J. **707**, 1131 (2009).
[37] S. Han and A. W. Steiner, Phys. Rev. C **96**, 035802 (2017).
[38] B.P. Abbott *et al.* (The LIGO Scientific Collaboration and the Virgo Collaboration), Phys. Rev. Lett. **121**, 161101 (2018).
[39] E. Flowers, M. Ruderman, and P. Sutherland, Astrophys. J. **205**, 541 (1976).
[40] M. E. Gusakov, A. D. Kaminker, D. G. Yakovlev, and O. Y. Gnedin, Astron. Astrophys. **423**, 1063 (2004).
[41] L. B. Leinson and A. Perez, arXiv:astro-ph/0606653.
[42] L. B. Leinson and A. Pérez, Phys. Lett. B **638**, 114 (2006).
[43] E. E. Kolomeitsev and D. N. Voskresensky, Phys. Rev. C **77**, 065808 (2008).
[44] A. W. Steiner and S. Reddy, Phys. Rev. C **79**, 015802 (2009).
[45] J. M. Lattimer, Annu. Rev. Nucl. Part. Sci. **62**, 485 (2012).
[46] B. Kiziltan, A. Kottas, M. D. Yoreo, and S. E. Thorsett, Astrophys. J. **778**, 66 (2013).
[47] F. Ozel and P. Freire, Annu. Rev. Astron. Astrophys. **54**, 401 (2016).
[48] A. R. Raduta, A. Sedrakian, and F. Weber, Mon. Not. R. Astron. Soc. **475**, 4347 (2018).
[49] R. Negreiros, L. Tolos, M. Centelles, A. Ramos, and V. Dexheimer, Astrophys. J. **863**, 104 (2018).
[50] A. Y. Potekhin, and G. Chabrier, Astron. Astrophys. **609**, A74 (2018).
[51] D. D. Ofengeim and D. G. Yakovlev, Mon. Not. R. Astron. Soc. **467**, 3598 (2017).
[52] M. V. Beznogov, E. Rrapaj, D. Page, and S. Reddy, Phys. Rev. C **98**, 035802 (2018).
[53] D. Blaschke, G. Röpke, H. Schulz, A. D. Sedrakian, and D. N. Voskresensky, Mon. Not. R. Astron. Soc. **273**, 596 (1995).
[54] C. Schaab, D. Voskresensky, A. D. Sedrakian, F. Weber, and M. K. Weigel, Astron. Astrophys. **321**, 591 (1997).
[55] P. S. Shternin, M. Baldo, and P. Haensel, Phys. Lett. B **786**, 28 (2018).
[56] M. Dutra, O. Lourenço, J. S. Sá Martins, A. Delfino, J. R. Stone, and P. D. Stevenson, Phys. Rev. C **85**, 035201 (2012).

[57] A. W. Steiner, J. M. Lattimer, and E. F. Brown, Eur. Phys. J. A **52**, 18 (2016).
[58] J. P. W. Verbiest, J. M. Weisberg, A. A. Chael, K. J. Lee, and D. R. Lorimer, Astrophys. J. **755**, 39 (2012).
[59] C. O. Heinke, P. G. Jonker, R. Wijnands, and R. E. Taam, Astrophys. J. **660**, 1424 (2007).
[60] M. V. Beznogov and D. G. Yakovlev, Mon. Not. R. Astron. Soc. **447**, 1598 (2015).
[61] M. V. Beznogov and D. G. Yakovlev, Mon. Not. R. Astron. Soc. **452**, 540 (2015).
[62] D. D. Ofengeim and D. A. Zyuzin, Particles **1**, 194 (2018).
[63] W. R. Hix, E. J. Lentz, E. Endeve, M. Baird, M. A. Chertkow, J. A. Harris, O. E. B. Messer, A. Mezzacappa, S. Bruenn, and J. Blondin, AIP Advances **4**, 041013 (2014).
[64] A. Burrows, Rev. Mod. Phys. **85**, 245 (2013).
[65] G. A. Lalazissis, J. König, and P. Ring, Phys. Rev. C **55**, 540 (1997).
[66] C. J. Horowitz and J. Piekarewicz, Phys. Rev. Lett. **86**, 5647 (2001).
[67] B. Nerlo-Pomorska and J. Sykut, Int. J. Mod. Phys. **E13**, 75 (2004).
[68] B. G. Todd-Rutel and J. Piekarewicz, Phys. Rev. Lett. **95**, 122501 (2005).
[69] F. J. Fattoyev, C. J. Horowitz, J. Piekarewicz, and G. Shen, Phys. Rev. C **82**, 055803 (2010).
[70] J. D. McDonnell, N. Schunck, D. Higdon, J. Sarich, S. M. Wild, and W. Nazarewicz, Phys. Rev. Lett. **114**, 122501 (2015).